Colloids and Surfaces B: Biointerfaces 236 (2024) 113832

Contents lists available at ScienceDirect

Colloids and Surfaces B: Biointerfaces

journal homepage: www.elsevier.com/locate/colsurfb

Understanding the petal effect: Wetting properties and surface structure of natural rose petals and rose petal-derived surfaces

Sergio Parra-Vicente [a], Pablo F. Ibáñez-Ibáñez [a], Miguel Cabrerizo-Vílchez [a], Isabel Sánchez-Almazo [b], Miguel Ángel Rodríguez-Valverde [a], Francisco Javier Montes Ruiz-Cabello [a,*]

[a] Laboratory of Surface and Interface Physics, Department of Applied Physics, University of Granada, Campus de Fuentenueva, Granada ES-18071, Spain
[b] Centro de Instrumentación Científica, Universidad de Granada, Granada, Spain

ARTICLE INFO

Keywords:
Petal surfaces
Drop retention
Templating
PDMS nanocasting
Surface heterogeneities

ABSTRACT

The petal effect is identified as a non-wetting state with high drop adhesion. The wetting behavior of petal surfaces is attributed to the papillose structure of their epidermis, which leads to a Cassie-Baxter regime combined with strong pinning sites. Under this scenario, sessile drops are pearl shaped and, unlike lotus-like surfaces, firmly attached to the surface. Petal surfaces are used as inspiration for the fabrication of functional para-hydrophobic surfaces such as antibacterial or water-harvesting surfaces. In this work, two types of rose petals were replicated by using a templating technique based in Polydimethylsiloxane (PDMS) nanocasting. The topographic structure, the condensation mechanism under saturated environments and the wetting properties of the natural rose petal and their negative and positive replicas were analyzed. Finally, we performed prospective ice adhesion studies to elucidate whether petal-like surfaces may be used as deicing solutions.

1. Introduction

Natural surfaces inspire since decades the development of functional surfaces because of their outstanding optical [1,2], chemical [3], thermal [4] and wetting properties [5]. Barthlott and Neinhuis [6] justified the self-cleaning and extreme water-repelling performance of lotus leaves (lotus effect) by their papillose epidermis [7] revealed through electron microscopy. Mimicking the low adhesion properties of lotus leaves has been widely reported [8–10]. However, incorporating the surface features that decorate the lotus leaves, or similar non-wettable natural surfaces is a challenging task. Lotus-like surfaces generally hold a double scale structure, which is difficult to reproduce at nano-scale. There is still a vivid debate regarding the chemical properties of lotus leaves and other lotus-like aerial plants. In most cases, the inner plant epidermis is intrinsically hydrophilic but plants can also secrete nanometer-sized waxes decorating its surface with hydrophobic nanoasperities.

Beyond the lotus leaves, other plant surfaces reveal singular wetting properties as well [11,12]. Feng et al. described the wetting of rose petals as a state of adhesive superhydrophobicity, namely the petal effect [13]. Water sessile drops formed on these hydrophobic surfaces are pearl-shaped (contact angle higher than 140º) but, unlike the lotus-like surfaces, the drop mobility is very low because the drops remain fixed to the sticky surface, even when the petal is flipped upside down. The origin of petal effect is still open. It is widely assumed that, just as for lotus-like surfaces, a double-scale structure is required for the petal effect. However, some authors have pointed out that a dual scale structure is not mandatory to reach a petal effect [14,15]. The wettability differences between petals are explained by the different size, shape and spacing of their micro-sized asperities [13]. The high contact angle is justified by the high roughness and the Cassie-Baxter regime. However, the larger solid-liquid contact area and the higher number of pinning sites along the contact line would explain the high drop adhesion on petal-like surfaces.

The fabrication of lotus-like or petal-like coatings requires firstly the incorporation of topographic features at different scales. This step is usually followed by a hydrophobization process if the substrate is intrinsically hydrophilic. However, it is still unclear whether the surface hydrophobicity is required to achieve both the lotus and petal effects. Some authors demonstrated that lotus leaves must be intrinsically hydrophobic because the direct replication of the structure of lotus leaf over hydrophilic substrates is unable to reach to superhydrophobicity [16,17]. This disagrees with others works in which the wettability of the cuticular waxes decorating superhydrophobic surfaces was analyzed,

* Correspondence to: Applied Physics Department, Faculty of Sciences, Campus de Fuentenueva, Granada E-18071, Spain.
E-mail address: fjmontes@ugr.es (F.J.M. Ruiz-Cabello).

https://doi.org/10.1016/j.colsurfb.2024.113832
Received 12 January 2024; Received in revised form 13 February 2024; Accepted 2 March 2024
Available online 4 March 2024

concluding that their intrinsic contact angle is lower than 90º [18,19]. Concerning the petal effect, it was assumed that the roughness in combination with a low energy surface are responsible for the high adhesion and high contact angles [13]. However, more recently, the petal effect has been explained in terms of chemical heterogeneity as well [20]. In other works, a high hydrophobicity is even not recommendable for petal effects [21].

Sun et al. [22] were able to fabricate an artificial lotus leaf by soft-lithography (nanocasting), curing Polydimethylsiloxane (PDMS) on natural lotus leaves. The negative replicas were used as templates to further fabricate the positive replicas. The surface features created on these positive replicas maintained the identical surface structure and wetting properties to the natural templates. The same strategy was followed by other authors [23–28] to replicate the surface structures of other plants with unique wetting properties. In most cases, the positive replicas maintained the same wetting properties as the natural template, but the negative replicas could behave differently.

PDMS surfaces have been proposed as anti-icing material due to their low ice adhesion and high robustness [29,30], both enhanced by the hydrophobicity and elasticity of the silicone-base material. In addition, the low thermal conductivity of PDMS was also connected to its ability to delay freezing [31].

In this work, we studied the surface structure, wetting properties and condensation ability of natural rose petals. The wetting properties were explored in terms of contact angle, drop retention and bouncing drop experiments. The surface topography was analyzed by confocal microscopy but the surface structure and micro-condensation by Environmental Scanning Electronic Microscope (ESEM). We also fabricated negative and positive replicas of the rose petals by surface templating (soft-lithography) with PDMS. The surface structure, surface topography and wettability of the negative and positive replicas were also analyzed. Once we were able to produce microstructured PDMS-based surfaces, we probed their anti-icing performance.

2. Materials and methods

2.1. Rose collection and sample preparation

Two different roses were purchased (local supplier): a red rose, namely Freedom Rose (FR) original from Ecuador and a cultivar yellow Rose, namely Mariyo Rose (MR), original from the Netherlands. Both roses were selected because of their wetting properties. We deposited small water droplets (around 10 μL in volume) on their petal surfaces and confirmed their high contact angle and low mobility, since pearl-like drops remained attached to the rose petal when it was flipped. It is worth to mention that the petal effect was not noticeable on all the rose petal surfaces explored. Instead, on some rose petals, although the drop contact angle was clearly high (surely higher than 140º), a high mobility was also observed: the drops easily rolled off at low inclination angles (lower than 5º). This behavior was identified as lotus effect, rather than petal effect.

For the double replication of the fresh rose petals, they were placed in the bottom of a petri dish. Once fixed with a double-side adhesive tape., they were gently flattened by softly pressing it against the petri dish with clean microscope coverslips. Subsequently, a 10:1 (v/v) mixture of PDMS and curing agent (Sylgard 184, Dow Corning) was poured into the petri dish, to cover the entire petal. The curing process was conducted at room temperature for 72 hours in an air-evacuated chamber aimed to remove the bubbles created during the mixing process. The negative replica was peeled-off and a Scotch tape was used to remove the petal residuals still attached to the replica. Then the PDMS sample was cleaned in toluene rinsed with water and let it dry at room temperature. The samples used for ESEM imaging or to fabricate the positive replicas were metallized by sputtering a thin carbon layer of thickness typically 2–20 nm. This metallization prior replication is needed for peeling the positive replica from the negative one and due to the low thickness of the layer deposited on the sample (~10 nm) it did not alter their roughness and structural properties. We initially tried to follow the same strategy than other authors [22], in which an antistick layer of trimethylchlorosilane was deposited on the PDMS surfaces for the fabrication of the positive replica, buy it failed. The positive replicas were also cleaned in toluene. This way, for each plant surface, we fabricated few negative and positive replicas. An scheme of the protocol used for the rose petals templating is illustrated in the supplementary information (see Figure S1). For comparison, smooth PMDS surfaces were also fabricated by replicating the bottom of plastic petri dishes. These sample were further cleaned as the replica surfaces. All the samples used for contact angle measurements were drilled with a small hole to form drops from below in the growing-shrinking sessile drop experiments [32].

2.2. Roughness measurements and surface morphology analysis

The roughness and surface topography of the native surfaces and their negative and positive PDMS replicas were analyzed by White-Light Confocal Microcopy (Plμ-Sensofar). In order to provide a parameter that serves to compare the roughness We focused on the Roughness factor (Ra) that was averaged over at least three individual topographies, at different locations on each sample. The selected magnification was 50X, the scanned area (285 × 210) μm^2, and the z-step was fixed to 0.2 μm.

The surface morphology of the petals and their replicas was also analyzed by ESEM (Thermofisher, Quanta 650 FEG) at high vacuum using an ETD detector working at 5KV. With this aim, the rose petals were fixed using a 2.5% solution of glutaraldehyde in cacodylate. Subsequently they were dehydrated in different ethanol concentrations (50%, 70%, 80%, 90%, 95%, 100%). Finally, the samples were subjected to critical point drying process with CO_2 using a Leica EM CPD300 apparatus. The petal surfaces and their replicas were coated with carbon (EMITECH K975X) to make them electroconductive.

2.3. Contact angle, bouncing drop and critical tilting angle measurements

The contact angles were measured with the growing-shrinking method based on Axisymmetric Drop Shape Analysis- Profile (ADSA-P). These experiments were carried out as follows: a seed drop of 20 μL in volume was deposited over the surface by using a micropipette covering the small hole that was previously drilled on the sample. Then, the drop was grown from below by using a microinjector (Hamilton, PSD-3) at a rate of 2 μL/s, until the drop volume reached 200 μL. Subsequently, the drop was shrinked until the drop volume decreased down to its initial volume of 20 μL. Drop side views were captured with a digital camera at 1fps. Each image was further analyzed by ADSA-P to determine the drop contact angle and contact radius. These experiments were used to determine the Advancing Contac Angle (ACA) and the Receding Contact Angle (RCA) by averaging the contact angle observed when the contact line was advancing or receding over the surface, respectively. The Bouncing Drops experiments were conducted similarly as reported elsewhere [33]. These experiments are aimed to determine the number of bounces of a water drop of volume (4.0 ± 0.2) μL released from a height of (10.1 ± 0.2) mm. The entire sequence is recorded with a high-speed camera (Phantom Miro 4), capturing 4200 images per second with an exposure time of 235 μs and delay between captures of 3 μs. The Critical Tilting Angle (CTA) was measured by using a Tilting plate instrument, described elsewhere [34]. This angle is defined as the minimum inclination angle for which a global motion of the drop is observed. This parameter is directly connected to the drop mobility: a high CTA (values typically higher than 30º) are associated to low mobile drops. However, the CTA value depends on drop volume. The range of drop volumes used in this study was 20 μL to 100 μL. Several surfaces used in this study were petal-like surfaces, then small drops were firmly pinned to the surface and no drop motion was observed, even when they are vertically tilted, or inverted upside down. For those

parahydrophobic surfaces, the tilting plate experiments required to use 100 μL drops for sliding.

2.4. Ice adhesion tests

The ice adhesion strength of the fabricated PDMS surfaces was measured by shear and tensile adhesion tests. These experiments were conducted as follows: a Teflon hollow cylindrical piece of inner radius ~10 mm (area ~78 mm^2) was placed on top of each sample and slightly pressed down to ensure no water leak. An amount of 1 mL of Milli-Q water was then poured inside the cylinder and the sample is introduced inside a freezing chamber for 90 min at −10ºC to ensure the total water freezing. The sample was then firmly fixed to a platform. Depending on the test adhesion mode, the platform is placed horizontally (for tensile adhesion tests) or vertically (for shear adhesion tests). When conducting tensile adhesion tests, the cylinder is connected to the force gauge by using a robust string. The gauge pulls up the cylinder perpendicularly to the surface. For shear adhesion tests, the cylinder is also connected to the gauge by a string but, in this case, they are pulled up parallel to the surface with the applying force point separated 1 mm from the surface. The force is applied by a digital force gauge (ZTA-200 N, ZTA Series) which monitors the force applied at each gauge-sample separation distance in a rate of 10 mm/min. During each sequence, the force increases generally linearly upon distance until the ice is suddenly separated from the surface. From this moment on, the force drops to zero. The maximum measured force is defined as the rupture force or ice release force, and it may be used to determine the ice adhesion strength by normalizing this force value by the contact area.

2.5. Micro-condensation analysis on fresh rose petals by ESEM

The ESEM working in variable pressure mode allowed us to observe the rose samples under simulated humid environmental conditions. A Peltier device attached to the ESEM stage is used to control and stabilize the sample temperature at around 2 °C. The samples are equilibrated at this temperature for about 15 minutes before the chamber is evacuated. The chamber is purged twice during the evacuation process. To reach 100% relative humidity (RH), the water pressure in the chamber was increased to 5.3 Torr and once this pressure is stabilized, the water starts to condense on the samples. To stabilize the water condensation process and facilitate the image capture, the temperature was lowered to 0ºC, and the chamber pressure was set to 4.6 Torr, while maintaining 100% relative humidity. Images were obtained at an accelerating voltage of 10 kV using the gaseous electron secondary detector (GSED) with a differential aperture of 500 μm. The thermal isolating properties of PDMS surfaces delayed condensation substantially. It impeded to reproduce the same experiments on the replicas as well as the smooth PDMS sample (control).

3. Results

3.1. Wettability analysis of the samples

The wettability properties of the raw rose petals, their negative replicas (-), their positive replicas (+) and the smooth PDMS sample (control) were first explored in terms of water contact angle. The results are displayed in Fig. 1. We noticed that both types of rose behave as petal-like surfaces, as expected. This was reflected in the high CAH (> 60º) and high ACA (>140º) in both cases. The differences between roses were found in the RCA values, since the one for the Freedom Rose (~80º) was noticeably higher than the one for the MR (~60º). However, the differences between the negative replicas of both roses were remarkable. The negative replica of the Freedom rose petal illustrates a lotus-like surface, since both the ACA and RCA values were high (142º and 120º, respectively). In contrast, the negative replica of the MR petal showed even a higher CAH (~90º) than the one observed for the natural petal

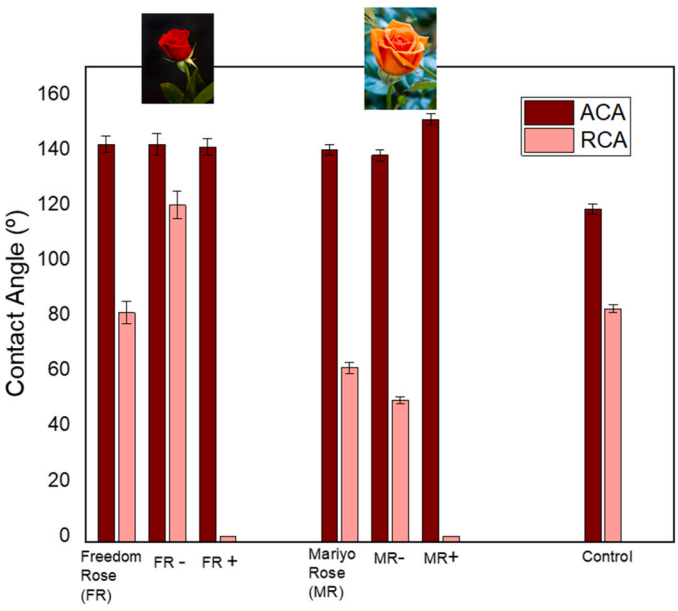

Fig. 1. Advancing Contact Angle (ACA) and Receding Contact Angle (RCA) for all the samples prepared in this study. The left bars correspond to a natural Freedom Rose petal (FR), its negative PDMS replica (FR-) and its positive PDMS replica (FR+). The central bars correspond to a natural Mariyo rose petal (MR), its negative PDMS replica (MR-) and its positive PDMS replica (MR+). The right bars correspond a smooth PDMS surface used as control.

surface used as template (~80º). Concerning the positive replicas, both samples showed much higher CAH (>140º). It was revealed by the absence of drop receding during the measurements. This might be explained by the high intrinsic CAH of PDMS, evidenced in the smooth PDMS with low surface roughness (CAH ~35º). It is worth noting that both petals and all their replicas. regardless of whether they are positive or negative, showed similar ACA values, but different RCA values.

The Critical Tilting Angle (CTA) values for all the used samples are shown in Table 1. For these experiments, we had to use large water drops (100 μL) because this drop size ensured the sliding/rolling-down on all the tilted samples. Most of the surfaces used were petal-like surfaces, then with volume ≤50 μL were pinned. The CTA confirm the CAH results. The natural petal surfaces and their positive replicas were identified as petal-like surfaces because their CTA values were high (>18º). However, the negative replicas of both petals behave differently. The Freedom Rose negative replica (FR -) showed a low CTA value(~5º), connected to lotus-like surfaces, while the negative replica of the Mariyo Rose (MR -) revealed a high CTA value (~49º). The positive replicas prepared showed an enhanced petal effect, with higher values of CTA, in comparison with the original template surfaces. We also notice that, despite its low roughness, the control PDMS sample was adhesive, as

Table 1
Critical Tilting angle, Number of bounces and Average Roughness (Ra) measured for each sample used in this work.

Sample	Critical Tilting Angle (º)	Number of Bounces	Ra (μm)
Freedom Rose (FR)	18.2±1.3	1±1	6.7±0.6
FR -	5.3±0.7	5±1	8.3±0.3
FR+	36.9±1.4	1±1	5.9±0.6
Mariyo Rose (MR)	31±3	0	5.2±0.6
MR +	49±2	0	3.9±0.3
MR -	54±2	0	3.2±0.2
PDMS control	28.0±1.2	0	0.036 ±0.017

indicated by its high CTA (~28º). This explains the magnification of petal effect on the positive replicas based on PMDS.

The bouncing drop experiments (see Table 1) allowed to confirm that only the negative replica of the rose petal acts as a lotus-like surface (~4 bounces). The rest of the surfaces were not water repellent.

In order to understand the petal effect, we conducted tilting plate experiments by using different drops volumes, varying from 20 μL to 100 μL, on three different samples: the original FR petal, the original MR petal and the smooth PDMS sample (control), for comparison. In Fig. 2, we analyze how the CTA varies as the drop volume. In accordance with our previously mentioned results, the FR petal is less adhesive than the MR petal throughout (see Fig. 2a). However, in both cases we found a strong dependence on volume, unlike the smooth PDMS sample. This suggests that the drop retention is promoted by the surface asperities, rather than the intrinsic chemical heterogeneity of the material. This finding evidenced that the petal effect is identified as a strong drop adhesion but particularly noticeable for small drops (<10 μL), while large drops may move on the surface upon certain driving forces (e.g., gravity or wind). In Fig. 2b, we show the results for similar experiments carried out with the negative and positive replicas of the FR petals. We compare these results with the natural FR petal. None drop displacement

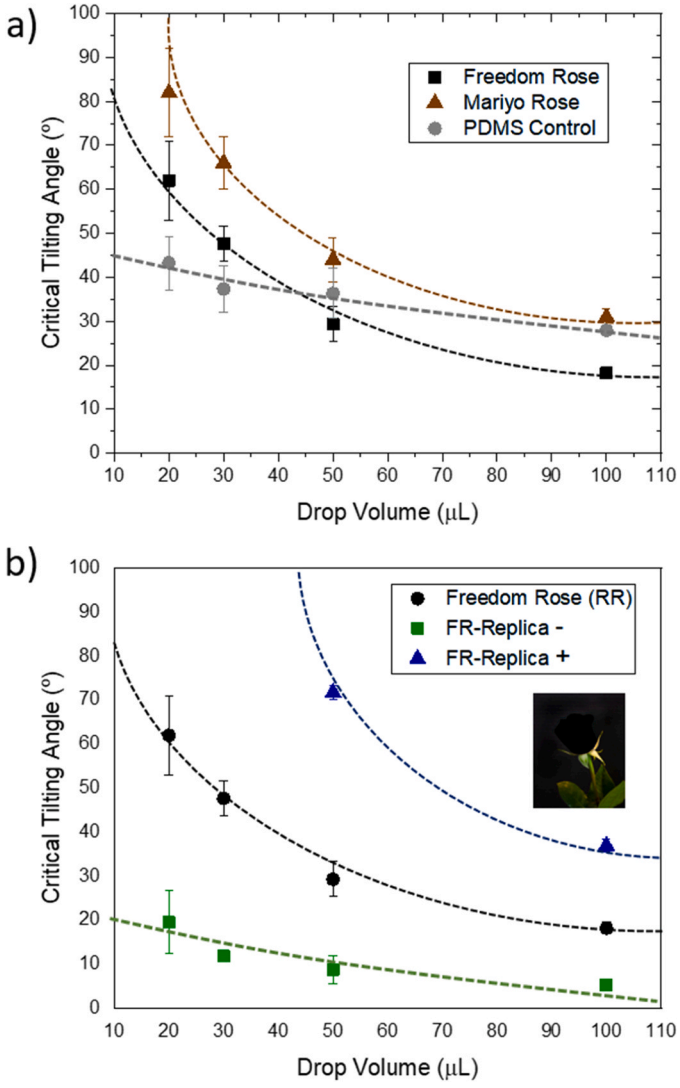

Fig. 2. Critical Tilting Angle in terms of the drop volume. In (a), we plot the results for a natural red rose, a natural Mariyo Rose (MR) and a smooth PDMS sample used as control, for comparison. In (b) we show the results for a natural red rose, its negative replica and positive replica.

was observed on the positive replica for drop volume lower than 50 μL. This high adhesive state was also observed on the MR petal because this petal and their replicas were even more sticky than the FR petal (results are not shown in this Figure). With the results shown in Fig. 2b, we noticed that the drop adhesion on the FR petal is not reproduced on its negative replica. The CTA values are low over the entire range of volumes and the volume dependence was less remarkable. We confirm that the negative replica behaved as a lotus-like surface, rather than a petal-like surface. However, the FR positive replica was highly adhesive for both small and large drops and the drop volume dependence was steeper.

3.2. Roughness measurements and surface morphology analysis

The results of Ra are also displayed in Table 1. The natural rose petals have in general similar Ra values than their replicas, as expected. However, it is worth mentioning that the negative replica of the FR petal is rougher than its original template. This was unexpected since the surface replication usually produces slightly smoother samples. We noticed that some petal pieces were attached to the negative replica after it was detached from the original template. Although the macroscopic remains were peeled off by using a scotch tape, some microscopic traces might still alter the surface roughness. In Table 1, it is also remarkable that the smooth PDMS sample has a submicron-scale roughness, which contrast with the rest of the samples.

The morphology of the structured surfaces (the natural petals and their replicas) at different magnifications was analyzed by ESEM. This information is shown as supplementary information (see Figure S2) we show the surface morphology of the rose petals at three different Horizontal Field Width (HFW). The petal surface is fully covered by a papillose structure. Each cell has a polygonal shape of length 10–30 μm and is covered by a wrinkle-like structure composed by elongated nanometric asperities, mainly distributed on the upper part of the cells. The main differences between the two roses are the compactness of the cells and their spacing. The epidermis cells of the FR petal have convex shape and are more confined than the ones on the MR petal. These features may explain the wettability properties of the petal surfaces and their replicas. The lower RCA value and higher CTA value of the MR petal is likely attributed to the higher contact area between the drop and the petal surface, which reduces the presence of air pockets and increases the number of pinning sites.

In Fig. 3, we compare the surface structure of both rose petals with their negative and positive replicas. It is noticeable that the surface templating reproduced both the microstructure and the cell nanostructure, at certain level. However, these nanoasperities were softened with respect to the natural petals. This explains why the CAH is much higher for the positive replicas in comparison to their original templates. The wetting behavior of the FR negative replica is justified by the compactness of the cells, as illustrated in Figure S3 (see Supplementary Information). The direct replication of the FR petal provides a surface with structure reminiscent of a wasp nest (see inset in Figure S2), where the pores (size typically 20–30 μm) were created by each single cell. For the FR petal, the cell spacing is small and hence the negative replica consists of confined pores separated by thin borders (size typically 1–2 μm). For this reason, the contact area between sessile drops and the surface of the FR negative replica is minimized, leading to lotus effect. The larger cell spacing on the MR petal justifies the wider pore borders in their negative replicas. This increases the drop contact area, and therefore, its adhesion to the substrate.

3.3. Ice adhesion

The deicing performance of all the PDMS samples prepared in this study were analyzed by ice adhesion tests. We explored the shear and tensile ice release force. These results are displayed in Fig. 4a. This Figure shows that the microstructure of the replicas is detrimental to the

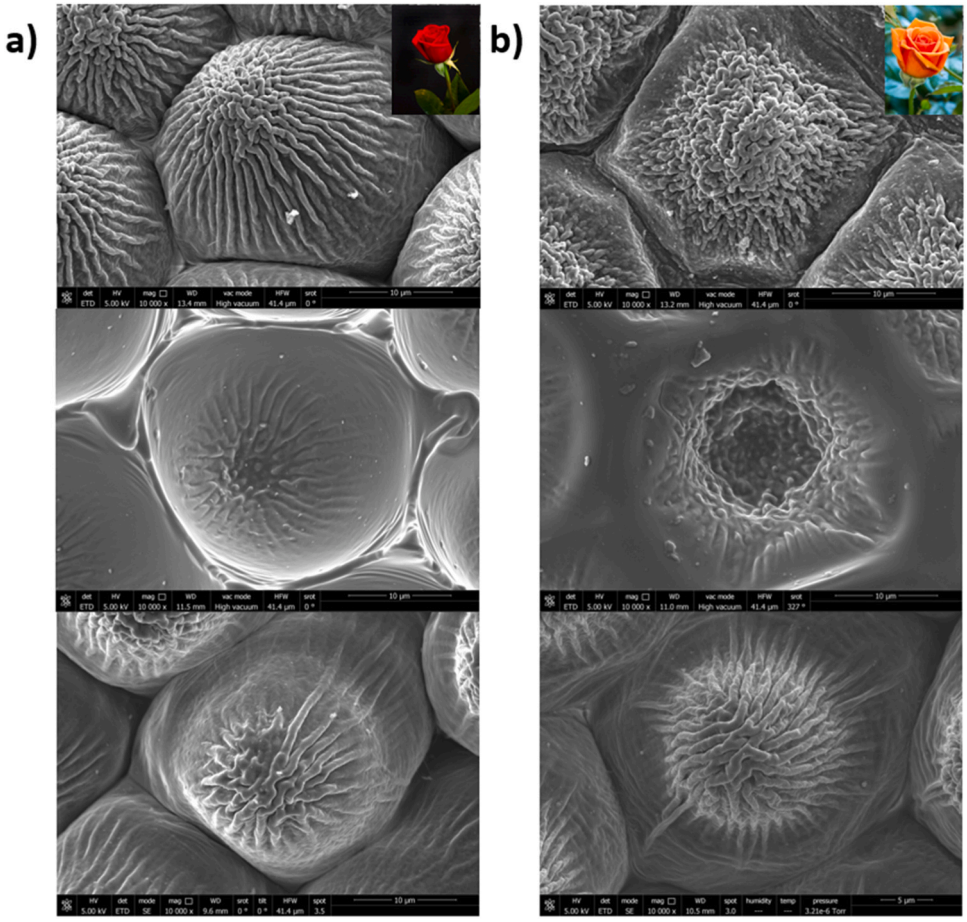

Fig. 3. ESEM images, acquired using an Horizontal Field Width (HFW) of 41.4 μm, of (top) the natural rose petals, (middle) their negative replicas and (bottom) their positive replicas. The images in the column (a) correspond to the Freedom Rose (FR) petals and the images in the column (b) to the Mariyo Rose (MR) petal.

deicing properties, because the ice adhesion for the smoothest sample is clearly lower than the one for the rest of samples. This is expected because, in our work, most of the microstructured PDMS samples act as petal-like surfaces. A high water (drop) adhesion should lead to high ice adhesion as well. However, the negative replica of the FR petal showed the lowest drop adhesion, revealed by the low CTA over the entire range of drop volumes (see Fig. 4b) and the highest ice adhesion, particularly the tensile adhesion. The high ice adhesion of certain lotus-like surfaces is justified mechanically rather than thermodynamically, by the so-called mechanical interlocking [35]. The shape and distribution of the pores on the negative replica of the rose petal could enhance this effect because water that partially penetrates the pores is later trapped once it freezes. As illustrated in Fig. 4b, the force applied to detach ice from the surface produces, not only an adhesive/cohesive failure, but also a surface deformation aimed to overcome the mechanical interlocking. The differences found between both replicas of the MR petals are not so pronounced, explained by a lower convexity of their micropapillae. The positive replica of the FR petal is slightly more adhesive than the positive replica of the MR petal. This difference can be attributed to the higher surface roughness (see Table 1) of the former one.

3.4. Microcondensation on natural rose petals

The water condensation mechanism on natural rose petals was analyzed by ESEM operating at a humid environment (100% relative humidity). In Fig. 5, we show microscopic images, acquired at different magnifications, aimed to explore the drop formation and the condensed drop shape under saturating conditions. In Fig. 5a, we show a sequence from the early stage of condensation (top image) to few seconds later (bottom image). During the early condensation, the drops were formed preferentially on the surface valleys, i.e., the spacing between micropapillae. However, small droplets are simultaneously formed on top of the micropapillae ridges. Once the condensation process is more advanced, the growing drops come into contact and coalesce. They form larger drops with contact lines pinned at the micropapillae peaks. Meanwhile, the water accumulated on the valleys percolated thorough cavities between cells (wicking effect).

There are two different regimes of water condensation on the natural petals: nucleating valleys and nucleating peaks. As previous studies [33, 36] reported, those structured high-energy surfaces reveal a bottom-up water filling under humid environments. However, this behavior is opposite to low-energy surfaces, for which the drops are mainly formed and grown on the peaks and the valleys are void. This condensation process typically comes out with sessile drops at the Cassie-Baxter regime.

The top image in Fig. 5b shows a pearl–shaped drop formed on the top of a micropapilla and it suggests that this domain of the petal is intrinsically hydrophobic, i.e. the papilla ridge is hydrophobic. However, the bottom image in Fig. 5b shows a drop formed in the spacing between five micropapillae and its contact line rests on the lower part of each one. The contact angle in this case reveals less hydrophobicity on this surface domain. This local wettability analysis points out to the plausible chemical heterogeneity of rose petals, reported by other authors [20]The mixed water condensation captures the paradrophobicity of rose petals.

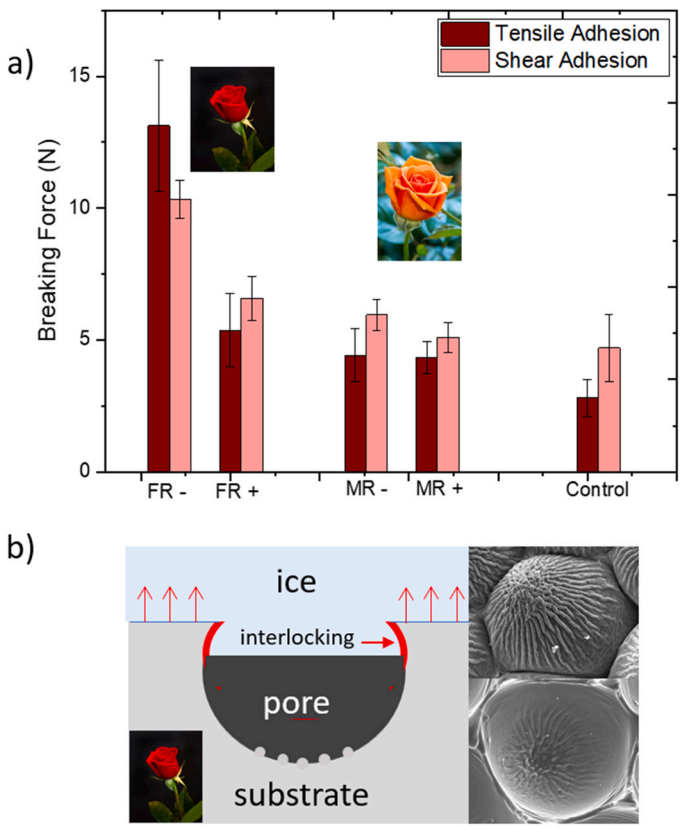

Fig. 4. (a) Ice Release force measured for all the PDMS samples used in this work: a Freedom rose negative replica (FR -), a red rose positive replica (FR+) a Mariyo rose negative replica (MR-), its positive replica (MR +) and a smooth sample (Control). (b) illustration of the mechanical interlocking that explains the high values of breaking force for the porous FR- sample.

4. Conclusions

In this work, several replicas of two different rose petals were satisfactory fabricated by a templating process based in PDMS nanocasting [22]. The negative replicas were produced by nanocasting the original petal, while the positive replicas are fabricated by a further replication using the negative replica as template. The samples were characterized in terms of wetting properties, surface structure analysis, roughness measurements, deicing performance and microcondensation analysis by ESEM.

A full analysis of the wetting properties of the raw rose petals revealed that this behavior cannot be simply defined as a superhydrophobic state with high adhesion, as pointed out by some authors [13]. Our results revealed that the petal effect might be also connected to a noticeable size dependence. These surfaces were not sticky to large drops (>10 μL) but, they were very sticky for small drops (< 10 μL). It means that the petal effect enables water retention as well as self-cleaning. However, the PDMS replicas obtained in this work were parahydrophobic but with retention over the entire range of volumes (even for large drops). This apparent enhancement of the petal effect, understood in terms of contact angle and CAH, was attributed to the high intrinsic CAH of PDMS and the limitation of the nanocasting technique to reproduce the petal nanoasperities. The structure of the negative replica, fabricated by templating the natural rose petals, is composed by ordered and confined pores which spacing, and convexity are crucial to understand the wetting behavior of the resulting surface. When the petal micropapillae are confined and their shapes are hemispherical (rose petal), the negative replica is covered by a dense pore distribution with thick borders. These replica surfaces are water-repellent as lotus-like surfaces, especially for large drops. These results disagree with other studies in which the negative replicas, and the positive replicas, are both considered petal-like surfaces [23]. This apparent discrepancy is due to the volume of the drops used for the wettability analysis (typically lower than 10 μL). The deicing properties of the produced samples was explored by ice shear and tensile adhesion tests. The microstructured PDMS surfaces are not suitable for anti-icing purposes. In all cases, the adhesion strength was higher than the one measured for a smooth PDMS surface, used as control sample. We

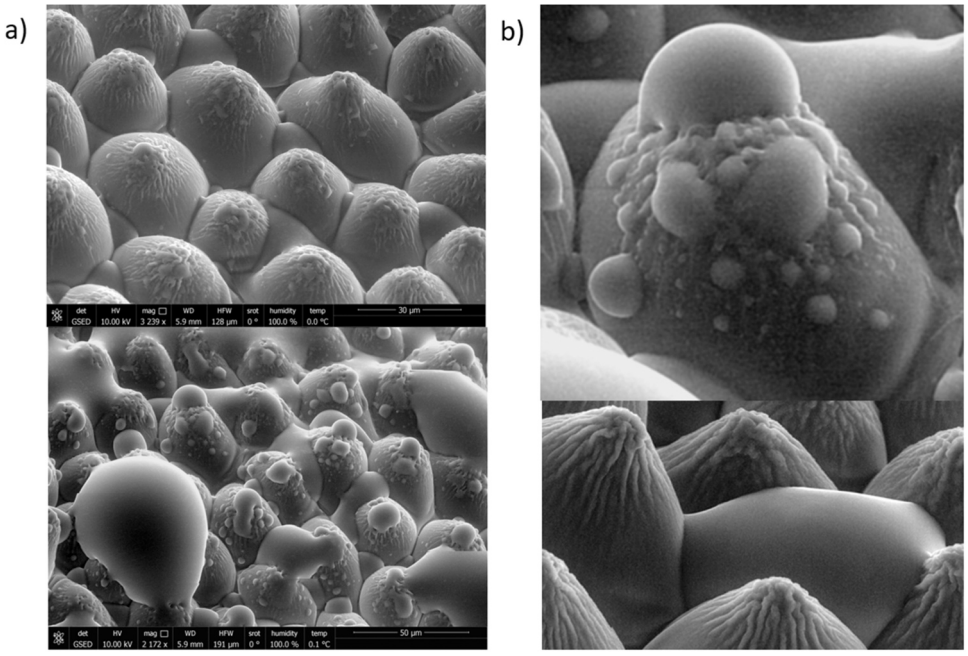

Fig. 5. ESEM images of a Freedom Rose petal under saturating conditions. Figure (a) shows the early condensation (top) and the late condensation (bottom). (b) Drops found on a saturated surface (top) initially formed on the micropapillae ridges or (bottom) the space between micropapillae.

noticed that the surface with the highest ice adhesion, also showed the lowest water affinity. This confirms the findings reported by other authors [35] in which superhydrophobic surfaces, especially those fabricated by the incorporation of microcavities, are deficient solutions as anti-icing agents. Considering the water condensation analysis on a raw/native real petal, we found that the rose petals showed a dual condensation mechanism most likely attributed to the presence of intrinsically hydrophilic and hydrophobic domains. The nucleation sites were found to be, simultaneously, the micropapillae ridges and the spacing between these micropapillae. It is well known that the surface peaks are more favorable nucleation sites on hydrophobic surfaces [33], while the valleys are considered as preferential nucleation sites on microstructured hydrophilic surfaces [36]. The condensation analysis pointed out to a plausible chemical heterogeneity of the rose petals. This analysis was not reproduced on the positive replicas because the low thermal conductivity of PDMS [31] hindered the radiative dew condensation on this material. The microscale analysis of the wettability properties of rose petal, conducted by ESEM, revealed the hydrophobicity of the micropapillae apex, while they hydrophilicity of their lateral surface, which explains the above mentioned two different condensation mechanisms. The surface heterogeneity of the rose petals has been recently reported by other authors [20]. This hybrid behavior shows the complex and outstanding properties of rose petal surfaces. The fabrication of perfect rose petal-like surfaces deserves the exploration to other alternatives because the properties of a rose petal cannot be only achieved by reproducing finely their surface structure. Further work should be addressed to combine the incorporation of the double scale structure and chemical heterogeneity and to understand in detail the petal effect and their potential applications.

CRediT authorship contribution statement

Sergio Parra-Vicente: Validation, Investigation. **Miguel Cabrerizo-Vílchez:** Validation, Resources, Methodology, Funding acquisition. **Pablo Ibáñez-Ibáñez:** Validation, Supervision, Methodology, Investigation. **Miguel Ángel Rodríguez-Valverde:** Writing – review & editing, Validation, Supervision, Project administration, Funding acquisition, Formal analysis, Conceptualization. **Isabel Sánchez-Almazo:** Writing – review & editing, Methodology, Investigation. **Francisco Javier Montes Ruiz-Cabello:** Writing – original draft, Validation, Supervision, Resources, Project administration, Methodology, Investigation, Funding acquisition, Formal analysis, Conceptualization.

Declaration of Competing Interest

The authors declare the following financial interests/personal relationships which may be considered as potential competing interests: Francisco Javier Montes Ruiz-Cabello reports was provided by University of Granada. If there are other authors, they declare that they have no known competing financial interests or personal relationships that could have appeared to influence the work reported in this paper.

Data availability

No data was used for the research described in the article.

Acknowledgements

This work was supported by the project PID2020–116082GB-I00 funded by MCIN/ AEI/10.13039/501100011033. P.F.I.I. acknowledges the funding from the Margarita Salas grant (Ministerio de Universidades, Next Generation EU). Authors want to acknowledge to Lola Molina Fernández, from the Scientific Photography Unit of the University of Granada, for coloring the image that was used in the graphical abstract. Funding for open access charge: Universidad de Granada/ CBUA.

Appendix A. Supporting information

Supplementary data associated with this article can be found in the online version at doi:10.1016/j.colsurfb.2024.113832.

References

[1] R. Xiong, J. Luan, S. Kang, C. Ye, S. Singamaneni, V. v Tsukruk, Biopolymeric photonic structures: design, fabrication, and emerging applications, Chem. Soc. Rev. 49 (2020) 983–1031, https://doi.org/10.1039/C8CS01007B.
[2] B. Fritz, R. Hünig, M. Guttmann, M. Schneider, K.M.S. Reza, O. Salomon, P. Jackson, M. Powalla, U. Lemmer, G. Gomard, Upscaling the fabrication routine of bioreplicated rose petal light harvesting layers for photovoltaic modules, Sol. Energy 201 (2020) 666–673, https://doi.org/10.1016/j.solener.2020.03.020.
[3] M. Qin, M. Sun, R. Bai, Y. Mao, X. Qian, D. Sikka, Y. Zhao, H.J. Qi, Z. Suo, X. He, Bioinspired hydrogel interferometer for adaptive coloration and chemical sensing, Adv. Mater. 30 (2018) 1800468, https://doi.org/10.1002/adma.201800468.
[4] S. Metwally, S. Martínez Comesaña, M. Zarzyka, P.K. Szewczyk, J.E. Karbowniczek, U. Stachewicz, Thermal insulation design bioinspired by microstructure study of penguin feather and polar bear hair, Acta Biomater. 91 (2019) 270–283, https://doi.org/10.1016/j.actbio.2019.04.031.
[5] J.S. George, P. Vijayan P, A.T. Hoang, N. Kalarikkal, P. Nguyen-Tri, S. Thomas, Recent advances in bio-inspired multifunctional coatings for corrosion protection, Prog. Org. Coat. 168 (2022) 106858, https://doi.org/10.1016/j.porgcoat.2022.106858.
[6] W. Barthlott, C. Neinhuis, Purity of the sacred lotus, or escape from contamination in biological surfaces, Planta 202 (1997) 1–8, https://doi.org/10.1007/s004250050096.
[7] C. Neinhuis, W. Barthlott, Characterization and distribution of water-repellent, self-cleaning plant surfaces, Ann. Bot. 79 (1997) 667–677, https://doi.org/10.1006/anbo.1997.0400.
[8] S. Chen, M. Zhu, Y. Zhang, S. Dong, X. Wang, Magnetic-responsive superhydrophobic surface of magnetorheological elastomers mimicking from lotus leaves to rose petals, Langmuir 37 (2021) 2312–2321, https://doi.org/10.1021/acs.langmuir.0c03122.
[9] C. Chen, M. Liu, L. Zhang, Y. Hou, M. Yu, S. Fu, Mimicking from rose petal to lotus leaf: biomimetic multiscale hierarchical particles with tunable water adhesion, ACS Appl. Mater. Interfaces 11 (2019) 7431–7440, https://doi.org/10.1021/acsami.8b21494.
[10] D. Wang, J. Huang, Z. Guo, Tomato-lotus inspired edible superhydrophobic artificial lotus leaf, Chem. Eng. J. 400 (2020) 125883, https://doi.org/10.1016/j.cej.2020.125883.
[11] R. Feng, C. Xu, F. Song, F. Wang, X.-L. Wang, Y.-Z. Wang, A bioinspired slippery surface with stable lubricant impregnation for efficient water harvesting, ACS Appl. Mater. Interfaces 12 (2020) 12373–12381, https://doi.org/10.1021/acsami.0c00234.
[12] S.G. Lee, H.S. Lim, D.Y. Lee, D. Kwak, K. Cho, Tunable anisotropic wettability of rice leaf-like wavy surfaces, Adv. Funct. Mater. 23 (2013) 547–553, https://doi.org/10.1002/adfm.201201541.
[13] L. Feng, Y. Zhang, J. Xi, Y. Zhu, N. Wang, F. Xia, L. Jiang, Petal effect: a superhydrophobic state with high adhesive force, Langmuir 24 (2008) 4114–4119, https://doi.org/10.1021/la703821h.
[14] K.-Y. Yeh, K.-H. Cho, Y.-H. Yeh, A. Promraksa, C.-H. Huang, C.-C. Hsu, L.-J. Chen, Observation of the rose petal effect over single- and dual-scale roughness surfaces, Nanotechnology 25 (2014) 345303, https://doi.org/10.1088/0957-4484/25/34/345303.
[15] H.-P. Lin, L.-J. Chen, Direct observation of wetting behavior of water drops on single micro-scale roughness surfaces of rose petal effect, J. Colloid Interface Sci. 603 (2021) 539–549, https://doi.org/10.1016/j.jcis.2021.06.132.
[16] D.M. Spori, T. Drobek, S. Zürcher, M. Ochsner, C. Sprecher, A. Mühlebach, N. D. Spencer, Beyond the lotus effect: roughness influences on wetting over a wide surface-energy range, Langmuir 24 (2008) 5411–5417, https://doi.org/10.1021/la800215r.
[17] W. Li, A. Amirfazli, Hierarchical structures for natural superhydrophobic surfaces, Soft Matter 4 (2008) 462–466, https://doi.org/10.1039/B715731B.
[18] Y.T. Cheng, D.E. Rodak, C.A. Wong, C.A. Hayden, Effects of micro- and nano-structures on the self-cleaning behaviour of lotus leaves, Nanotechnology 17 (2006) 1359, https://doi.org/10.1088/0957-4484/17/5/032.
[19] P. Wagner, R. Fürstner, W. Barthlott, C. Neinhuis, Quantitative assessment to the structural basis of water repellency in natural and technical surfaces, J. Exp. Bot. 54 (2003) 1295–1303, https://doi.org/10.1093/jxb/erg127.
[20] L. Almonte, C. Pimentel, E. Rodríguez-Cañas, J. Abad, V. Fernández, J. Colchero, Rose petal effect: A subtle combination of nano-scale roughness and chemical variability, Nano Sel. 3 (2022) 977–989, https://doi.org/10.1002/nano.202100193.
[21] T. Darmanin, F. Guittard, A one-step electrodeposition of homogeneous and vertically aligned nanotubes with parahydrophobic properties (high water adhesion), J. Mater. Chem. A Mater. 4 (2016) 3197–3203, https://doi.org/10.1039/C5TA09253A.
[22] M. Sun, C. Luo, L. Xu, H. Ji, Q. Ouyang, D. Yu, Y. Chen, Artificial lotus leaf by nanocasting, Langmuir 21 (2005) 8978–8981, https://doi.org/10.1021/la050316q.
[23] S. Dai, Y. Zhu, Y. Gu, Z. Du, Biomimetic fabrication and photoelectric properties of superhydrophobic ZnO nanostructures on flexible PDMS substrates replicated from

rose petal, Appl. Phys. A 125 (2019) 138, https://doi.org/10.1007/s00339-019-2438-7.
[24] N. Ghosh, A. Bajoria, A.A. Vaidya, Surface chemical modification of poly (dimethylsiloxane)-based biomimetic materials: oil-repellent surfaces, ACS Appl. Mater. Interfaces 1 (2009) 2636–2644, https://doi.org/10.1021/am9004732.
[25] J.-J. Hwang, C.-Y. Wu, Y.-H. Hung, M.-X. Li, K.-H. Luo, H.-W. Jia, J.N.I. Balitaan, S.-R. Lin, J.-M. Yeh, Biomimetic PMMA coating surface and its application on inhibition of bacterial attachment and anti-biofilm performance, Surf. Interfaces 36 (2023) 102548, https://doi.org/10.1016/j.surfin.2022.102548.
[26] U.U. Ghosh, S. Nair, A. Das, R. Mukherjee, S. DasGupta, Replicating and resolving wetting and adhesion characteristics of a Rose petal, Colloids Surf. A Physicochem Eng. Asp. 561 (2019) 9–17, https://doi.org/10.1016/j.colsurfa.2018.10.028.
[27] Y. Cao, S. Jana, L. Bowen, X. Tan, H. Liu, N. Rostami, J. Brown, N.S. Jakubovics, J. Chen, Hierarchical rose petal surfaces delay the early-stage bacterial biofilm growth, Langmuir 35 (2019) 14670–14680, https://doi.org/10.1021/acs.langmuir.9b02367.
[28] C.-M. Chang, Z.-H. Hu, T.-Y. Lee, Y.-A. Huang, W.-F. Ji, W.-R. Liu, J.-M. Yeh, Y. Wei, Biotemplated hierarchical polyaniline composite electrodes with high performance for flexible supercapacitors, J. Mater. Chem. A Mater. 4 (2016) 9133–9145, https://doi.org/10.1039/C6TA01781A.
[29] P.F. Ibáñez-Ibáñez, F.J. Montes Ruiz-Cabello, M.A. Cabrerizo-Vílchez, M. A. Rodríguez-Valverde, Ice adhesion of PDMS surfaces with balanced elastic and water-repellent properties, J. Colloid Interface Sci. 608 (2022) 792–799, https://doi.org/10.1016/j.jcis.2021.10.005.
[30] C. Chen, Z. Tian, X. Luo, G. Jiang, X. Hu, L. Wang, R. Peng, H. Zhang, M. Zhong, Micro–nano-nanowire triple structure-held PDMS superhydrophobic surfaces for robust ultra-long-term icephobic performance, ACS Appl. Mater. Interfaces 14 (2022) 23973–23982, https://doi.org/10.1021/acsami.2c02992.
[31] F.J. Montes Ruiz-Cabello, S. Bermúdez-Romero, P.F. Ibáñez-Ibáñez, M. A. Cabrerizo-Vílchez, M.A. Rodríguez-Valverde, Freezing delay of sessile drops: Probing the impact of contact angle, surface roughness and thermal conductivity, Appl. Surf. Sci. 537 (2021) 147964, https://doi.org/10.1016/j.apsusc.2020.147964.
[32] F.J.M. Ruiz-Cabello, M.A. Rodríguez-Valverde, M.A. Cabrerizo-Vilchez, Contact angle hysteresis on polymer surfaces: an experimental study, J. Adhes. Sci. Technol. 25 (2011), https://doi.org/10.1163/016942410×544848.
[33] F.J.M. Ruiz-Cabello, P.F. Ibáñez-Ibáñez, J.F. Gómez-Lopera, J. Martínez-Aroza, M. Cabrerizo-Vílchez, M.A. Rodríguez-Valverde, Testing the performance of superhydrophobic aluminum surfaces, J. Colloid Interface Sci. 508 (2017), https://doi.org/10.1016/j.jcis.2017.08.032.
[34] F.J.M. Ruiz-Cabello, M.A. Rodríguez-Valverde, M. Cabrerizo-Vílchez, A new method for evaluating the most stable contact angle using tilting plate experiments, Soft Matter 7 (2011), https://doi.org/10.1039/c1sm06196h.
[35] J. Chen, J. Liu, M. He, K. Li, D. Cui, Q. Zhang, X. Zeng, Y. Zhang, J. Wang, Y. Song, Superhydrophobic surfaces cannot reduce ice adhesion, Appl. Phys. Lett. 101 (2012) 111603, https://doi.org/10.1063/1.4752436.
[36] M. Yarom, A. Marmur, Condensation enhancement by surface porosity: three-stage mechanism, Langmuir 31 (2015) 8852–8855, https://doi.org/10.1021/acs.langmuir.5b02003.